MEK1 and MEK2 differentially control the duration and amplitude of the ERK cascade response

Pawel Kocieniewski[1] **and Tomasz Lipniacki**[1,2]

[1]Institute of Fundamental Technological Research, Polish Academy of Sciences, 02-106 Warsaw, Poland

[2]Department of Statistics, Rice University, Houston, TX 77025, USA

E-mail: tlipnia@ippt.gov.pl

Abstract. The Raf/MEK/ERK cascade is one of the most studied and important signal transduction pathways. However, existing models largely ignore the existence of isoforms of the constituent kinases and their interactions. Here, we propose a model of the ERK cascade that includes heretofore neglected differences between isoforms of MEK. In particular, MEK1 is subject to a negative feedback from activated ERK, which is further conferred to MEK2 via heterodimerization. Specifically, ERK phosphorylates MEK1 at the residue Thr292, hypothetically creating an additional phosphatase binding site, accelerating MEK1 and MEK2 dephosphorylation. We incorporated these recently discovered interactions into a mathematical model of the ERK cascade that reproduces the experimental results of Catalanotti *et al* 2009 (*Nat Struct Mol Biol* **16** 294–303) and Kamioka *et al* 2010 (*J Biol Chem* **285** 33540–8). Furthermore, the model allows for predictions regarding the differences in the catalytic activity and function of the MEK isoforms. We propose that MEK1/MEK2 ratio regulates the duration of the response, which increases with the level of MEK2 and decreases with the level of MEK1. In turn, the amplitude of the response is controlled by the total amount of the two isoforms. We confirm the proposed model structure performing a random parameter sampling, which led us to the conclusion that the sampled parameters, selected to properly reproduce wild-type (WT) cells behavior, qualitatively reproduce differences in behavior WT cells and cell mutants studied experimentally.

Keywords: MAPK cascade, kinase isoforms, MEK1–MEK2 heterodimer, negative feedback, rule-based modeling, random parameter sampling.

PACS numbers: 87.14.E-, 87.15.km, 87.16.A-, 87.16.Xa, 87.18.Mp, 87.18.Vf

1. Introduction

The Raf/ERK pathway belongs to the MAPK family and is important in regulating proliferation and differentiation. Its core comprises three levels of kinases, Raf (MAP3K), MEK (MAP2K), and ERK (MAPK), activated sequentially upon growth factors stimulation [1]. Signal transduction through the pathway culminates in bisphosphorylation and activation of ERK, which subsequently translocates into the nucleus. The time profile of the ERK phosphorylation, its localization (cytoplasmic vs. nuclear) as well as the cell type determine the ultimate physiological response to the signal (proliferation/differentiation/survival). Interestingly, the components of the ERK pathway possess isoforms. Specifically, the Raf family comprises A-, B-, and C-Raf. The MEK family includes MEK1, MEK1b (a splice variant), and MEK2 [2]. Similarly, the ERK family comprises ERK1, ERK1c, and ERK2 [3]. Each isoform is distinctively characterized in terms of regulation, activity, and expression pattern. In this study we will analyze regulatory consequences of the existence and differences of MEK isoforms, MEK1 and MEK2.

The MAPK cascades are involved in a number of malignancies. The p38 and JNK pathways play important roles in Alzheimer, Parkinson, and Lou-Gehrings diseases and have been implicated in cancer. Nonetheless, the ERK cascade plays a particularly prominent role in cancer. Oncogenic (usually activating) mutations in EGF receptor, K-Ras, N-Ras and Raf kinases (especially B-Raf) and other pathway components are frequent contributors to tumorigenesis [4]. However, the cascade's dysregulation also plays a causal role in a number of developmental disorders, collectively referred to as Neuro-Cardio-Facial-Cutaneous (NCFC) syndromes. These diseases are caused by germline mutations in the components of the pathway. They include neurofibromatosis type 1 as well as Noonan, LEOPARD, CFC, and Costello syndromes. The disorders are characterized by a combination of facial disfigurements, cardiac abnormalities, and diminished height, although cutaneous, genital and mental abnormalities are also common. The specific set of symptoms along with genetic analysis generally enable unambiguous diagnosis [5].

Many models of the MAPK pathway in general, and ERK cascade in particular have been published to date [7, 8]. The first model was published in 1996 by Huang and Ferrell who demonstrated the potential of the core cascade for ultrasensitive (switch-like) behavior [9]. This result has been later attributed to the distributive nature of the bisphosphorylation required for the activation of MEK and ERK. The switch-like behavior has been later experimentally demonstrated in *Xenopus* oocytes [10]. Subsequent models were characterized by larger complexity and explored different aspects of regulation. Kholodenko *et al* [11] focused on modeling EGF receptor signaling, demonstrating the importance of competition between different adaptor molecules in their interaction with EGF receptor while determining signaling response. Another model by Schoeberl *et al* [12] explored the role of the dynamics of receptor activation, internalization, and recycling on the cellular response to EGF. The model of Schoeberl

et al was latter incorporated into a larger model of ErbB receptor signaling by Chen *et al* [13], who showed that signal-response relation in the MAPK cascade is context-dependent. That is, the model displays steeper response when isolated than when embedded into a larger network. The regulation of temporal characteristics of the response (e.g. transient vs. sustained vs. oscillatory) as well as multistability have also been analyzed pointing to the importance of numerous feedbacks in the cascade [14, 15, 16, 17, 18]. The feedback to Raf has been found to be especially relevant to the pathway robustness by endowing the cascade with the properties of a Negative Feedback Amplifier [19]. Furthermore, the existence of the various negative feedbacks implied the cascade's potential for oscillation, which was indeed experimentally confirmed [20].

Nonetheless, the vast majority of the models have neglected differences between isoforms of the cascade components, even though they are prevalent at all its levels. To date, there has been a handful of models deliberately accounting for such differences. Specifically, two models incorporated differences between ERK1 and ERK2, demonstrating their physiological significance. In particular, Harrington *et al* [21] have shown how different nuclear trafficking rates of activated ERK1 and ERK2 can influence their cytoplasmic and nuclear distribution, hence physiological response. Schilling *et al* have demonstrated the interplay between ERK1 and ERK2 phosphorylation via the negative feedback, and their opposing roles in promoting cell proliferation [22]. In addition to the ERK1 and ERK2 specific models, Robubi *et al* [23] formulated a simple model that incorporated B-Raf and C-Raf, accounting for the differences in their activation/inactivation rates and catalytic activities. Their results have suggested that both isoforms are equally important in determining response intensity, but B-Raf is mostly responsible for regulating the duration of the response.

So far no model has considered the differences between MEK isoforms, MEK1 and MEK2, even though they clearly have non-redundant and non-compensatory functions in cell cycle regulation, carcinogenesis, and development [24, 25, 26, 27, 28, 29, 30, 31, 32, 33]. Most strikingly, MEK1-deficient mice die during embryonic development due to placental defects [34], while MEK2-deficient mice are viable [35]. Although MEK1 and MEK2 are highly homologous, being 80% similar in the overall sequence and 90% similar in their kinase domain, they display marked differences (52% similarity) in their main regulatory region, Proline Rich Domain (PRD) [2]. Specifically, MEK1 possesses phosphorylation sites in this region that are not found in MEK2 [36]. Relevant to our studies, MEK1 has a unique phosphorylation site (Thr292), that can be phosphorylated by ERK [37]. This phosphorylation presumably creates a MEK phosphatase binding site, accelerating MEK1 inactivation. As demonstrated by Catalanotti *et al* [38], this Thr292-dependent negative feedback regulation of MEK1 is conferred to MEK2 via heterodimerization. Based on these experimental findings, we have formulated a mathematical model of the ERK cascade.

The model contains all levels of the ERK cascade, and is implemented using the rule-based formalism of BioNetGen [39]. It successfully reproduces the results of Catalanotti *et al* 2009 [38] and Kamioka *et al* 2010 [40]. The model indicates

the importance of the MEK1/MEK2 ratio and MEK total content as regulators of the response duration and amplitude, respectively. We verified model structure by performing a random parameter sampling, which allowed us to demonstrate that the parameters which properly reproduce the wild-type (WT) cells responses, qualitatively reproduce the behaviors of four cell mutants studied by Catalanotti *et al* [38].

2. Model

The model has been implemented and simulated using BioNetGen — a rule-based specification language and environment [39]. In BioNetGen language (BNGL), models are constructed by specifying rules that describe allowed protein–protein interactions, processes, and covalent modifications. Based on the rules, the reaction network is automatically generated along with the system of ordinary differential equations. The advantage of this approach is that it often allows for more concise definition of models with large numbers of interactions and protein states. The model comprises the following 8 proteins (seed species): EGFR receptor, Sos1, Ras, Raf, MEK1 and MEK2, MEK-specific phosphatase (PHP), and ERK (figure 1). Their amounts were assumed within the ranges reported in the literature (see Table 2). These proteins interact according to 41 rules, and are subject to modifications, state transitions (active/inactive, ligand-bound/ligand-free) and complex formation, which lead to the generation of 110 species (including sink and source) and the equivalent number of ODEs. The model encompasses all levels of the Raf/MEK/ERK cascade, beginning with the EGF receptor activation by the ligand at the cell membrane to the activation of ERK. The annotated BioNetGen code is included in the Electronic Supplementary Material.

The binding rate of the EGFR ligand (c_1) is considered the input signal S_0. The level of activated (bisphosphorylated) ERK, ERK_{pp}, is considered the response of the cascade. The response is characterized by the following metrics (figure 2):

(i) **Peak Time** ($T_{\max}$) – the time required to achieve the maximal response.

(ii) **Relative Response Amplitude** ($R_{\max}$) – the maximal fraction of activated ERK: $R_{\max} = ERK_{\mathrm{pp}}(T_{\max})/ERK_{\mathrm{tot}}$.

(iii) **Response** (R_{t}) – response at time t normalized to the maximal response: $R_{\mathrm{t}} = ERK_{\mathrm{pp}}(t)/ERK_{\mathrm{pp}}(T_{\max})$. In this paper we consider R_{30} and R_{60}.

(iv) **Decay Time** ($T_{1/\mathrm{n}}$) – the time at which the response decreases to $(1/n)$-th of its maximal value.

Model Assumptions

The model contains the following mechanistic assumptions:

(i) In unstimulated cells receptor subunits exist as monomers, which undergo constitutive production and degradation [41].

(ii) The Epidermal Growth Factor (EGF) is assumed to be present at constant concentration during stimulation. Its depletion in the extracellular media due to receptor binding and receptor-mediated internalization is neglected.

(iii) Upon EGF binding, two EGF-bound EGFR monomers irreversibly dimerize and transphosphorylate [41, 42]. EGF binding is assumed to be irreversible.

(iv) EGF-bound phosphorylated protomer of the EGFR dimer can bind Sos1. EGFR-bound Sos1 is considered activated [43].

(v) EGFR dimer undergoes accelerated degradation together with any bound ligand and Sos1 molecules [44].

(vi) Active, EGFR-bound Sos1 catalyzes the transition of Ras-GDP to Ras-GTP (active Ras) [43].

(vii) Active Ras activates Raf kinase [6].

(viii) Active Raf kinase distributively phosphorylates MEK1 and MEK2 on their two Raf-dependent sites (RDS) [45]. Both sites need to be phosphorylated for the kinase to become and remain active [46]. Activated MEKs phosphorylate ERK.

(ix) MEK1 and MEK2 can homo- and heterodimerize [47]. The dimerization is stimulation-independent and does not affect their catalytic activity [38].

(x) The differences between ERK1 and ERK2 are neglected and both proteins are jointly represented as ERK. Active MEK1 and MEK2 distributively phosphorylate ERK. Both sites need to be phosphorylated for the kinase to become and remain active [48].

(xi) The model contains two negative feedback loops. Namely, active ERK phosphorylates (1) Sos1, preventing its association with the receptor [49], and (2) MEK1 (at Thr292) , creating a binding site for PHP [38].

The model parameters and assumed levels of all proteins are given in Tables 1 and 2. In Table 1 we also give information which of the four metrics (excluding $T_{1/n}$, which is to some extent redundant with R_{30} and R_{60}) is affected by changing the given parameter.

Negative Feedbacks

Catalanotti *et al* [38] have established the importance of the MEK1-based negative feedback. Active ERK phosphorylates MEK1 at Thr292 creating presumably a binding site for the MEK phosphatase, accelerating deactivation of MEK1. It is assumed that the MEK1-bound phosphatase can also dephosphorylate MEK2 if the latter is in the heterodimer with MEK1.

The ERK cascade contains several other negative feedback loops. However, for the sake of simplicity, we consider in our model only one additional feedback loop, namely, the canonical feedback loop to Sos1. Specifically, Sos1 undergoes feedback phosphorylation by active ERK. Phosphorylated Sos1 can no longer bind to the receptor dimer subunits and hence cannot be activated [49].

3. Results

3.1. Model compatibility with experimental data

The model successfully reproduces the experimentally observed time courses reported by Kamioka *et al* [40] and Catalanotti *et al* [38]. Specifically, Kamioka *et al* [40] have recorded the following time courses of the upstream components of the cascade: (1) the level of EGFR phosphorylation, (2) the level of Ras-GTP, and (3) the level of inhibited Sos1 due to ERK feedback phosphorylation. Our model satisfactorily reproduces these results (figure 3). The agreement with Kamioka *et al* [40] data on Ras-GTP ensures the correct input to the Raf/MEK/ERK module analyzed further in respect to the experiments by Catalanotti *et al* [38].

In particular, Catalanotti *et al* [38] have measured the phosphorylation time profiles of ERK phosphorylation and MEK pRDS in WT and transfected Mouse Embryonic Fibroblast (MEFs) cells. The expression of transfected mutant MEK1 proteins was assumed to be the same as of MEK1 in WT cells. MEK pRDS accounts for the combined MEK1 and MEK2 bisphosphorylation. The time course data were obtained from cells treated with Epidermal Growth Factor (EGF). These results motivated our study and are satisfactorily reproduced by the model. In the model, the experimental perturbations were achieved by modifying the appropriate rules or species concentrations. Specifically, the model reproduced the results of the following experiments:

(i) **Wild-type cells** (figure 4). ERK phosphorylation and MEK pRDS time profiles were recorded in MEFs obtained from WT mice in response to EGF stimulation. The response of WT cells was simulated using the default parameters and concentrations given in Table 1.

(ii) **Knock-out of MEK1** (figure 4). The corresponding time profiles were obtained for MEK1-deficient cells. In the model, MEK1 knock-out was simulated by setting MEK1 concentration to 0.

(iii) **Ablation of MEK1 homo- and heterodimerization** (figure 5). The ablation has been achieved by substituting Asp78 with glycine in the dimerization domain (MEK1 mutant N78G). This mutation was shown to disrupt MEK1 dimerization. This MEK1 mutant has been expressed in MEK1 deficient MEF cells. In the model, the ablation of MEK1 homo- and heterodimerization has been achieved by disabling the rules governing MEK1 dimerization.

(iv) **Ablation of the negative feedback from ERK to MEK1** (figure 6). This ablation has been achieved by substituting Thr292 with alanine (MEK1 mutant T292A), disabling the negative feedback phosphorylation. This MEK1 mutant has been expressed in MEK1-deficient MEF cells. In the model, T292A mutation has been modeled by disabling the rule specifying phosphorylation of Thr292 residue by ERK.

(v) **Constitutive MEK1 repression** (figure 7). The constitutive repression has been achieved by substituting Thr292 with aspartic acid (mutant T292D). Aspartic acid

is a phosphomimetic amino acid T292D mutation is supposed to recapitulate the effects of phosphorylation. This MEK1 mutant has been expressed in MEK1-deficient MEF cells. The T292D mutation has been modeled by assuming that threonine Thr292 is constitutively modified and binds MEK phosphatase with the same affinity as the phosphorylated residue in WT protein. This is the sole measurement by Baccarini group experiment [38] that is not well reproduced by the model. The experiment is puzzling in itself because the weak transient total MEK phosphorylation appeared to be followed by the prolonged ERK1/2 activation. Very recently, the same group of Baccarini (Zmajkovicova *et al* [50], figure 6d) demonstrated that in fact the ERK1/2 activity in T292D mutant cells remains at the basal level.

The foregoing analysis demonstrated the compatibility between the proposed model and experimental data. One should keep in mind that there exists large uncertainty about model parameters, and because of their redundancy (which arises when a change of two or more parameters has the same or opposite influence on output) this uncertainty may not be removed by fitting. Therefore, in order to support the proposed model structure, we validate the model based on random parameter sampling, see Appendix.

3.2. Model predictions

The mathematical model provides insight into the kinetics of individual MEK isoforms and their mutants, which cannot be experimentally discerned. Specifically, the model demonstrates different roles of the $MEK1/MEK2$ ratio and MEK total content MEK_{tot} in regulating the response amplitude and duration. It also allows for making predictions about the relative MEK1 and MEK2 catalytic activities, and the sensitivity of MEK1 T292D mutant responses. These predictions are discussed in detail below.

(i) **The impact of the $MEK1/MEK2$ ratio and MEK_{tot} on the response characteristics.** The increasing ratio of $MEK1/MEK_{\mathrm{tot}}$ (where $MEK_{\mathrm{tot}} = MEK1 + MEK2$) leads to a substantial decrease of the decay time, $T_{1/3}$, restricting the duration of the response (figure 8(B)). In contrast, $MEK1/MEK_{\mathrm{tot}}$ has a limited impact on the amplitude of the response $R_{\max}$ (figure 8(A)). Peak time $T_{\max}$ is also largely insensitive to this ratio; it increases only for the weak signal when the MEK1 content is small (figure 8(C)). For the weakest signal ($S = 0.01 \times S_0$) there is a discontinuity in $T_{\max}$ plotted as a function of $MEK1/MEK_{\mathrm{tot}}$. This discontinuity arises due to the existence of two local maxima in $ERK(t)$ profile. Time to peak is defined as the time to the global maximum in $ERK(t)$. For $MEK1/MEK_{\mathrm{tot}} < 0.1$ the global maximum is at $t \approx 40$ min; for $MEK1/MEK_{\mathrm{tot}} \approx 0.1$ the maximum at $t \approx 18$ min becomes higher, and thus time to peak changes abruptly from $t \approx 40$ min to $t \approx 18$ min at $MEK1/MEK_{\mathrm{tot}} \approx 0.1$. All analyzed response metrics exhibit higher dependence on $MEK1/MEK_{\mathrm{tot}}$ for low signals.

The response amplitude $R_{\max}$ increases with MEK_{tot} (figure 9). The $R_{\max}$ dependence on MEK2 level is stronger than the dependence to MEK1 level due to lower catalytic activity of the latter. The decay time $T_{1/3}$ increases with the MEK2 level and decreases with the MEK1 level (figure 9) confirming their opposite roles in system dynamics. Time $T_{1/3}$ becomes very long (> 1000 min) for the high level of MEK2 ($\geq 5 \times 10^5$) and correspondingly lower levels of MEK1. This shows the at high MEK_{tot}, response maybe not be terminated only when $MEK1 > MEK2$. The peak time $T_{\max}$ does not exhibit any unambiguous trend and generally $T_{\max}$ dependence on MEK1 and MEK2 levels is relatively modest, about two-fold between the extremes. $T_{\max}$ decreases with MEK1 level, and either decreases with MEK2 (for low MEK1 level), or increases (for high MEK1 level).

(ii) **Kinase activities of MEK1 and MEK2.** In our initial fitting we found that in order to reproduce the same amplitude of ERK activation in WT and MEK1-deficient cells, MEK2 kinase catalytic activity needed to be several fold (5-fold is assumed in our initial parameter set) greater than that of MEK1 (figure 10). The relaxation of this condition and assumption of the equal kinase activities lead to disagreement with the experimental time profiles for MEK1 KO and MEK1 N78G mutants. This result lends support to reports that MEK2 is in fact the stronger kinase in light of the inconsistencies in literature, where some groups found both MEK isoforms to be of equal activity [36, 11].

(iii) **Sensitivity of the MEK1 T292D transfected cell responses.** The analysis has shown that cells with T292D mutation exhibit highly sensitive responses to the level of MEK1 T292D mutant expression, while the responses of the other two mutants, T292A and N78G, are robust to the expression level (figure 10). We analyzed the influence of different mutant expression levels on the response for the three mutants, in the three-fold range around the WT expression level (assumed as default for all mutants). This can explain the differences between the two mentioned experiments on T292D mutant by the Baccarini group [38, 50].

4. Discussion

All of the constituent kinases of the ERK cascade possess isoforms characterized by specific functions and (cross-)interactions. We have constructed a mathematical model of the ERK cascade that accounts for the regulatory differences between MEK1 and MEK2 isoforms. Our hypothesis that MEK1-Thr292p is in fact a binding site has been recently supported by Zmajkovicova *et al* [50], where this residue was found to bind proteins containing WW domains. Thus MEK1-Thr292p can feasibly bind a phosphatase or phosphatase-containing inhibitory complex. Our model is in satisfactory agreement with the experimental data published the groups of Baccarini [38] and Matsuda [40]. Specifically, the model correctly reproduces the observed profiles of MEK and ERK activation obtained in the experiments with WT and perturbed MEFs. In particular, the model reproduces the prolonged activity of ERK and MEK due to the

ablation of the negative feedback to MEK1 by (1) MEK1 knockout, (2) mutation of the phosphatase binding site (MEK1 mutant T292A), and (3) disruption of MEK1/2 heterodimerization (MEK1 mutant N78G). As far as the effects of the phosphomimetic mutations are concerned (MEK1 mutant T292D), the experimental results have been variable. The original experiment [38] suggests weak and very transient MEK activation accompanied by some activity of ERK (different for ERK1 and ERK2 isoforms). On the other hand, the recent experiment by the same group of Baccarini ([50], figure 6d), published during the revision of the manuscript shows that in fact the ERK1/2 activity in T292D mutant cells remains almost at the basal level. In light of the performed sensitivity analysis, the observed discrepancy is no longer puzzling because constitutive repression introduces considerable sensitivity to the level of MEK1 T292D expression (which is difficult to control precisely in the experiment) in contrast to the other mutants.

Because of the variability of the reported levels of the MAPK kinase cascade components and kinetic rate constants, as well as the intrinsic heterogeneity of the MEF cell line, we have sought to verify the proposed model structure independently of a particular choice of parameters. Therefore, we repeated our analysis based on sampling parameter sets. Based on this analysis we demonstrated that for parameters sets sampled from *a posteriori* distribution (under the condition of proper reproduction of WT cell trajectories) the behavior of four cell mutants analyzed in [38] is satisfactorily reproduced. We believe that the proposed model validation method can be used for analysis of other models, whenever there exists large uncertainty about kinetic parameters such as in case of highly heterogeneous cell populations.

Our work provides insight into the role of the divergence of MEK1 and MEK2 isoforms in terms of regulation of signaling. We show how $MEK1/MEK2$ ratio and MEK total content regulate the duration and magnitude of ERK response, as first suggested by MEK1 KO experiments. The model suggests that this particular mode of regulations requires that MEK2 catalytic activity is several times greater than the activity of MEK1, however MEK1 content must be higher than that of MEK2 in order to allow for efficient repression of the latter. Given this, a picture emerges where MEK1 is responsible for restricting the duration of the ERK response and controlling the activity of its more potent counterpart.

Isoform-specific regulation is present at other levels of the cascade, especially at the level of Raf. In particular, B-Raf has significantly higher kinase activity than both A- and C-Raf. It possesses substantial basal activity, which upon stimulation increases 3-fold in comparison to 25-fold increase for C-Raf and A-Raf [51]. The isoforms further differ in their responses to negative feedback; B-Raf undergoes modest (33-50%) reduction in activity, while C-Raf activity rapidly decreases, and virtually disapperas by 30 min [52]. Similar to MEK1 and MEK2, Raf isoforms cross-regulate one another via dimerization, although these interactions are activating rather than inhibitory [6]. Complete understanding of the behavior of the ERK cascade will require inclusion of isoform-based regulation and future models should account for it.

5. Conclusions

Based on the experimentally supported model we found that the $MEK1/MEK2$ ratio controls the duration of the response, while the total amount of MEK isoforms MEK_{tot} governs the response amplitude. The decay time $T_{1/3}$ increases with the level of MEK2 and decreases with the level of MEK1. The peak time is largely robust to the MEK2 level and decreases with the MEK1 content. Based on these findings, we may conclude that ERK to MEK1 feedback has a distinctive role in negative regulation of the ERK cascade. In case of one-parametric feedback, increasing the strength of the feedback reduces both the amplitude and duration of the response. In our case, because the two MEK isoforms have opposing roles, the feedback enables almost independent regulation of the amplitude and duration of the response. Because there is a high variation of MEK1 and MEK2 levels between cell lines, one could expect different cell lines to respond differentially to the same growth factor stimulation.

Appendix: Model structure validation based on the random parameter sampling

The kinetic parameters, given in Table 1, were chosen to fit the data shown in figures 3 through 7. The parameter choice is not unique; there exists large redundancy, and a change in almost any parameter can be compensated by a corresponding change in one of its 'sibling' parameters (ones that have a similar, or opposite, impact on the observables). Moreover, one must remember that MEFs are not a well-defined, homogeneous cell line. Depending on a method of extraction, a MEF cell line contains a mixture of fibroblasts from different parts of embryos, which already display differential expression levels of the relevant genes. The matter is further complicated by a great variety of murine genetic backgrounds from which MEFs are isolated, contributing to the already considerable heterogeneity of cells used by different research groups. For this reason levels of the pathway components are expected to be significantly variable between experiments. Thus, in order to confirm the role of ERK to MEK1 (and MEK2) negative feeback, we performed analysis of the robustness of the model based on random parameter scan. In short, we sampled 5000 parameter sets from the cube extending three-fold below and above the default parameters values (Table 1). Using these sets of parameters, we simulated WT cells trajectories, and eliminated parameter sets for which bisphosphorylated ERK profile was in disagreement with the experimental data (based on the Catalanotti *et al* [38]). We consider four criteria: amplitude, time to peak, and response attenuation after 30 and 60 min). Using remaining 1116 sets of parameters (which can be considered parameter sets sampled from the *a posteriori* distribution that arises from an *a priori* distribution upon the condition of proper reproduction of the metrics of WT cells signaling), we simulated four perturbations (KO and 3 mutants). This allowed us to discern whether the difference between WT and mutant cell behavior results from the proposed model structure or only follows from the particular choice of

parameters.

The 31 parameters, given in upper part of Table 1, were sampled for each set. The input signal, default levels of Ras, Raf, MEK1, MEK2 and ERK, as well as EGFR and Sos1 synthesis and degradation rates (respectively s_1, d_1, s_2, and d_2), controlling steady state levels of EGFR and Sos1, as well as the parameters regulating MEKs homo- and heterodimerization (b_2, n_2, b_3, n_3, b_4, n_4) were assumed to be constant. Also the ratio of catalytic activities of MEK2 to MEK1 was left unchanged, equal 5. We uniformly sampled 5000 points (X_i, $i = 1...31$) from the 31-dimensional unit cube. Based on the obtained X_i, we calculated 5000 sets of new parameters K_i, as

$$K_\mathrm{i} = 3^{X_\mathrm{i}} \times k_\mathrm{i}, \tag{1}$$

where $X_\mathrm{i} \sim \mathcal{U}[-1, 1]$, k_i is the i^{th} default parameter, and $i = 1, ..., 31$.

Based on these sampled parameter sets (from *a priori* distribution), we simulated WT cells trajectories and eliminated these parameter sets for which at least one of four criteria was not satisfied. We choose the following criteria for determining compliant responses:

(i) Time to peak $T_{\max}$ should satisfy 3 min $< T_{\max} <$ 7 min.

(ii) Relative response amplitude should satisfy $R_{\max} > 0.6$.

(iii) Response at 30 min should satisfy $0.1 < R_{30} < 0.33$.

(iv) Response at 60 min should satisfy $R_{60} < 0.1$.

We provide scatter plots of $T_{\max}$ and $R_{\max}$ (figure 11) as well as R_{30} and R_{60} (figure 12), showing the WT cell values versus each cell mutant. The scatter plots were produced for 100 parameters sets out of 1116 sets satisfying the above criteria.

We found that $T_{\max}$ is relatively evenly distributed and peak occurs approximately 2 minutes later in mutated than in WT cells; the amplitude was also found relatively robust to the perturbations downregulating the negative feedback to MEK1 (KO, N78G, and T292A), figure 11. As expected, these perturbations lead to sustained activation of both MEK1 and ERK as indicated by the corresponding values for R_{30} and R_{60}. The ranges of these metrics are broad but in all cases both R_{30} and R_{60} exceed the values obtained for WT cells, figure 12. These results show that for parameters sampled from *a posteriori* distribution the simulated behavior of all mutants with downregulated negative feedback to MEK1 (KO, N78G, and T292A) qualitatively agrees with experiment. As far as constitutively repressed T292D MEK1 mutant is concerned, it exhibits similar distribution of $T_{\max}$ and R_{60} as the other mutants and predictably lower amplitudes in comparison to WT cells. In contrast, it displays significant heterogeneity in regard to R_{30}, indicating a wide range of potential time courses. Thus, this metric is very sensitive to the choice of parameter set.

The remaining 1116 (out of 5000) parameter sets represent *a posteriori* distribution. It is interesting how much the average parameter values (the averaging must be done in log-scale) obtained from this *a posteriori* distribution differ from the default values. Such averages may be considered as refined *centroid* parameters following from the assumed

default values and experimental constraints. In Table 1, we provide the default as well as the refined parameters; for most parameters the differences are very small, which implies that the initial choice of parameters is reasonable. The largest changes (*approx.* 5-20%) were observed for the parameters regulating strength of the MEK1-based negative feedback. In figures 13 and 14 we show $MEK_{\mathrm{pp}}(t)$ and $ERK_{\mathrm{pp}}(t)$ trajectories obtained for the default, averaged (refined), and 13 sampled parameter sets for WT cell and four cell mutants. As one could expect from parameter comparison, the trajectories obtained for the refined parameters do not differ substantially from those obtained for the default parameters, although (also as expected) they are more representative for trajectories obtained for the sampled parameters sets. Trajectories obtained for default, refined, but also sampled parameters (from *a posteriori* distribution) qualitatively fit experimental data obtained in Baccarini group experiment [38]. The MEK_{pp} and ERK_{pp} trajectories of KO, N78G, and T292A mutants are relatively robust, the T292D mutant trajectories are more variable, confirming high sensitivity of this mutant to parameters.

Acknowledgments

We thank Marek Kochańczyk for help in numerical simulations. This study was supported by the FNP grant TEAM/2009-3/6 and Polish National Science Center 2011/03/B/NZ2/00281.

Electronic Supplementary Material

BioNetGen codes allowing for simulation of WT cells and four mutants. The codes can be also used to generate MATLAB files.

References

[1] McKay M M, Morrison D K 2007 Integrating signals from RTKs to ERK/MAPK *Oncogene* **26** 3113–3121.

[2] Roskoski R Jr 2012 MEK1/2 dual-specificity protein kinases: structure and regulation *Biochem Biophys Res Commun* **417** 5–10.

[3] Roskoski R Jr 2012 ERK1/2 MAP kinases: structure, function, and regulation *Pharmacol Res* **66** 105–43.

[4] Kim E K , Choi E J 2010 Pathological roles of MAPK signaling pathways in human diseases *Biochim Biophys Acta* **1802** 396–405.

[5] Bentires-Alj M, Kontaridis M I, Neel B G 2006 Stops along the RAS pathway in human genetic disease *Nat Med* **12** 283–5.

[6] Roskoski R Jr 2010 RAF protein-serine/threonine kinases: structure and regulation *Biochem Biophys Res Commun* **399** 313–7.

[7] Orton R J, Sturm O E, Vyshemirsky V, Calder M, Gilbert D R, Kolch W 2005 Computational modelling of the receptor-tyrosine-kinase-activated MAPK pathway *Biochem J* **392** 249–61.

[8] Kholodenko B N, Birtwistle M R 2009 Four-dimensional dynamics of MAPK information processing systems *Interdiscip Rev Syst Biol Med* **1** 28–44.

[9] Huang C Y, Ferrell J E Jr 1996 Ultrasensitivity in the mitogen-activated protein kinase cascade *Proc Natl Acad Sci U S A* **93** 10078–83.

[10] Ferrell J E Jr, Machleder E M 1998 The biochemical basis of an all-or-none cell fate switch in Xenopus oocytes *Science* **280** 895–8.
[11] Kholodenko B N, Demin O V, Moehren G, Hoek J B 1999 Quantification of short term signaling by the epidermal growth factor receptor *J Biol Chem* **274** 30169–81.
[12] Schoeberl B, Eichler-Jonsson C, Gilles E D, Mller G 2002 Computational modeling of the dynamics of the MAP kinase cascade activated by surface and internalized EGF receptors *Nat Biotechnol* **20** 370–5.
[13] Chen W W, Schoeberl B, Jasper P J, Niepel M, Nielsen U B, Lauffenburger D A, Sorger P K 2009 Input-output behavior of ErbB signaling pathways as revealed by a mass action model trained against dynamic data *Mol Syst Biol* **5** 239.
[14] Kholodenko B N 2000 Negative feedback and ultrasensitivity can bring about oscillations in the mitogen-activated protein kinase cascades *Eur J Biochem* **267** 1583–8.
[15] Qiao L, Nachbar R B, Kevrekidis I G, Shvartsman S Y 2007 Bistability and oscillations in the Huang-Ferrell model of MAPK signaling *PLoS Comput Biol* **3** 1819–26.
[16] Sasagawa S, Ozaki Y, Fujita K, Kuroda S 2005 Prediction and validation of the distinct dynamics of transient and sustained ERK activation *Nat Cell Biol* **7** 365–73.
[17] Markevich N I, Hoek J B, Kholodenko B N 2004 Signaling switches and bistability arising from multisite phosphorylation in protein kinase cascades *J Cell Biol* **164** 353–359.
[18] Cirit M, Wang C C, Haugh J M 2012 Systematic quantification of negative feedback mechanisms in the extracellular signal-regulated kinase (ERK) signaling network *J Biol Chem* **285** 36736–44.
[19] Sturm O E, Orton R, Grindlay J, Birtwistle M, Vyshemirsky V, Gilbert D, Calder M, Pitt A, Kholodenko B, Kolch W 2010 The mammalian MAPK/ERK pathway exhibits properties of a negative feedback amplifier *Sci Signal* **3** 90
[20] Shankaran H, Wiley H S Oscillatory dynamics of the extracellular signal-regulated kinase pathway *Curr Opin Genet Dev* **20** 650–5.
[21] Harrington H A, Komorowski M, Beguerisse-Daz M, Ratto G M, Stumpf M P 2012 Mathematical modeling reveals the functional implications of the different nuclear shuttling rates of Erk1 and Erk2 *Phys Biol* **9** 036001.
[22] Schilling M, Maiwald T, Hengl S, Winter D, Kreutz C, Kolch W, Lehmann WD, Timmer J, Klingmller U 2009 Theoretical and experimental analysis links isoform-specific ERK signalling to cell fate decisions *Mol Syst Biol* **5** 334.
[23] Robubi A, Mueller T, Fueller J, Hekman M, Rapp U R, Dandekar T 2005 B-Raf and C-Raf signaling investigated in a simplified model of the mitogenic kinase cascade *Biol Chem* **386** 1165–71.
[24] Charron J, Bissonauth V, Nadeau V 2012 Implication of MEK1 and MEK2 in the establishment of the blood-placenta barrier during placentogenesis in mouse *Reprod Biomed Online* **25** 58–67.
[25] Zhou L, Tan X, Kamohara H, Wang W, Wang B, Liu J, Egami H, Baba H, Dai X 2010 MEK1 and MEK2 isoforms regulate distinct functions in pancreatic cancer cells *Oncol Rep* **24** 251–5.
[26] Scholl F A, Dumesic P A, Barragan D I, Harada K, Charron J, Khavari P A 2009 Selective role for Mek1 but not Mek2 in the induction of epidermal neoplasia *Cancer Res* **69** 3772–8.
[27] Voisin L, Julien C, Duhamel S, Gopalbhai K, Claveau I, Saba-El-Leil M K, Rodrigue-Gervais I G, Gaboury L, Lamarre D, Basik M, Meloche S 2008 Activation of MEK1 or MEK2 isoform is sufficient to fully transform intestinal epithelial cells and induce the formation of metastatic tumors *BMC Cancer* **8** 337.
[28] Skarpen E, Flinder L I, Rosseland C M, Orstavik S, Wierod L, Oksvold M P, Skalhegg B S, Huitfeldt H S 2008 MEK1 and MEK2 regulate distinct functions by sorting ERK2 to different intracellular compartments *FASEB J* **22** 466–76.
[29] Di Benedetto B, Hitz C, Hlter S M, Khn R, Vogt Weisenhorn D M, Wurst W 2007 Differential mRNA distribution of components of the ERK/MAPK signalling cascade in the adult mouse brain *J Comp Neurol* **500** 542–56.
[30] Ussar S, Voss T 2004 MEK1 and MEK2, different regulators of the G1/S transition *J Biol Chem*

279, 43861–9.

[31] Robinson F L, Whitehurst A W, Raman M, Cobb M H 2002 Identification of novel point mutations in ERK2 that selectively disrupt binding to MEK1 *J Biol Chem* **277** 14844–52.

[32] Alessandrini A, Brott B K, Erikson R L 1997 Differential expression of MEK1 and MEK2 during mouse development *Cell Growth Differ* **8** 505–11.

[33] Brott B K, Alessandrini A, Largaespada D A, Copeland N G, Jenkins N A, Crews C M, Erikson R L 1993 MEK2 is a kinase related to MEK1 and is differentially expressed in murine tissues *Cell Growth Differ* **4** 921–9.

[34] Giroux S, Tremblay M, Bernard D, Cardin-Girard J F, Aubry S, Larouche L, Rousseau S, Huot J, Landry J, Jeannotte L, Charron J 1999 Embryonic death of Mek1-deficient mice reveals a role for this kinase in angiogenesis in the labyrinthine region of the placenta *Curr Biol* **9** 369–72.

[35] Blanger L F, Roy S, Tremblay M, Brott B, Steff A M, Mourad W, Hugo P, Erikson R, Charron J 2003 Mek2 is dispensable for mouse growth and development *Mol Cell Biol* **23** 4778–87.

[36] Zheng C F, Guan K L 1993 Cloning and characterization of two distinct human extracellular signal-regulated kinase activator kinases, MEK1 and MEK2 *J Biol Chem* **268** 11435–9.

[37] Park E R, Eblen S T, Catling A D 2007 MEK1 activation by PAK: a novel mechanism *Cell Signal* **19** 1488–96.

[38] Catalanotti F, Reyes G, Jesenberger V, Galabova-Kovacs G, de Matos Simoes R, Carugo O, Baccarini M 2009 A Mek1-Mek2 heterodimer determines the strength and duration of the Erk signal *Nat Struct Mol Biol* **16** 294–303.

[39] Faeder J R, Blinov M L and Hlavacek W S 2009 Rule-based modeling of biochemical systems with BioNetGen *Meth Mol Biol* **500** 113–167.

[40] Kamioka Y, Yasuda S, Fujita Y, Aoki K, Matsuda M 2010 Multiple decisive phosphorylation sites for the negative feedback regulation of SOS1 via ERK *J Biol Chem* **285** 33540–8.

[41] Endres N F, Engel K, Das R, Kovacs E, Kuriyan J 2011 Regulation of the catalytic activity of the EGF receptor *Curr Opin Struct Biol* **6** 777–84.

[42] Hubbard S R, Mohammadi M, Schlessinger J 1998 Autoregulatory mechanisms in protein-tyrosine kinases *J Biol Chem* **273** 11987–90.

[43] Egan S E, Giddings B W, Brooks M W, Buday L, Sizeland A M, Weinberg R A 1993 Association of Sos Ras exchange protein with Grb2 is implicated in tyrosine kinase signal transduction and transformation *Nature* **363** 45–51.

[44] Burke P, Schooler K, Wiley H S Regulation of epidermal growth factor receptor signaling by endocytosis and intracellular trafficking 2001 *Mol Biol Cell* **6** 1897–910.

[45] Alessi D R, Saito Y, Campbell D G, Cohen P, Sithanandam G, Rapp U, Ashworth A, Marshall C J and Cowley S 1994 Identification of the sites in MAP kinase kinase-1 phosphorylated by p74raf-1 *EMBO J* **13** 1610–9.

[46] Zheng C F, Guan K L 1995 Activation of MEK family kinases requires phosphorylation of two conserved Ser/Thr residues *EMBO J* **5** 1123–31.

[47] Ohren J F, Chen H, Pavlovsky A, Whitehead C, Zhang E, Kuffa P, Yan C, McConnell P, Spessard C, Banotai C, Mueller W T, Delaney A, Omer C, Sebolt-Leopold J, Dudley D T, Leung I K, Flamme C, Warmus J, Kaufman M, Barrett S, Tecle H and Hasemann C A 2004 Structures of human MAP kinase kinase 1 (MEK1) and MEK2 describe novel noncompetitive kinase inhibition *Nat Struct Mol Biol* **11** 1192–7.

[48] Burack W R, Sturgill T W 1997 The activating dual phosphorylation of MAPK by MEK is nonprocessive *Biochemistry* **36** 5929–5933.

[49] Buday L, Warne P H, Downward J 1995 Downregulation of the Ras activation pathway by MAP kinase phosphorylation of Sos *Oncogene* **11** 1327–31.

[50] Zmajkovicova K, Jesenberger V, Catalanotti F, Baumgartner C, Reyes G, Baccarini M 2013 MEK1 Is Required for PTEN Membrane Recruitment, AKT Regulation, and the Maintenance of Peripheral Tolerance *Mol Cell* http://dx.doi.org/10.1016/j.bbr.2011.03.031, in press.

[51] Marais R, Light Y, Paterson H F, Mason C S, Marshall C J 1997 Differential regulation of Raf-1,

A-Raf, and B-Raf by oncogenic ras and tyrosine kinases *J Biol Chem* **272** 4378–83.

[52] Ritt D A, Monson D M, Specht S I, Morrison D K 2010 Impact of feedback phosphorylation and Raf heterodimerization on normal and mutant B-Raf signaling *Mol Cell Biol* **30** 806–19.

[53] Hatakeyama M, Kimura S, Naka T, Kawasaki T, Yumoto N, Ichikawa M, Kim J H, Saito K, Saeki M, Shirouzu M, Yokoyama S, Konagaya A 2003 A computational model on the modulation of mitogen-activated protein kinase (MAPK) and Akt pathways in heregulin-induced ErbB signalling Biochem J. **373** 451–63.

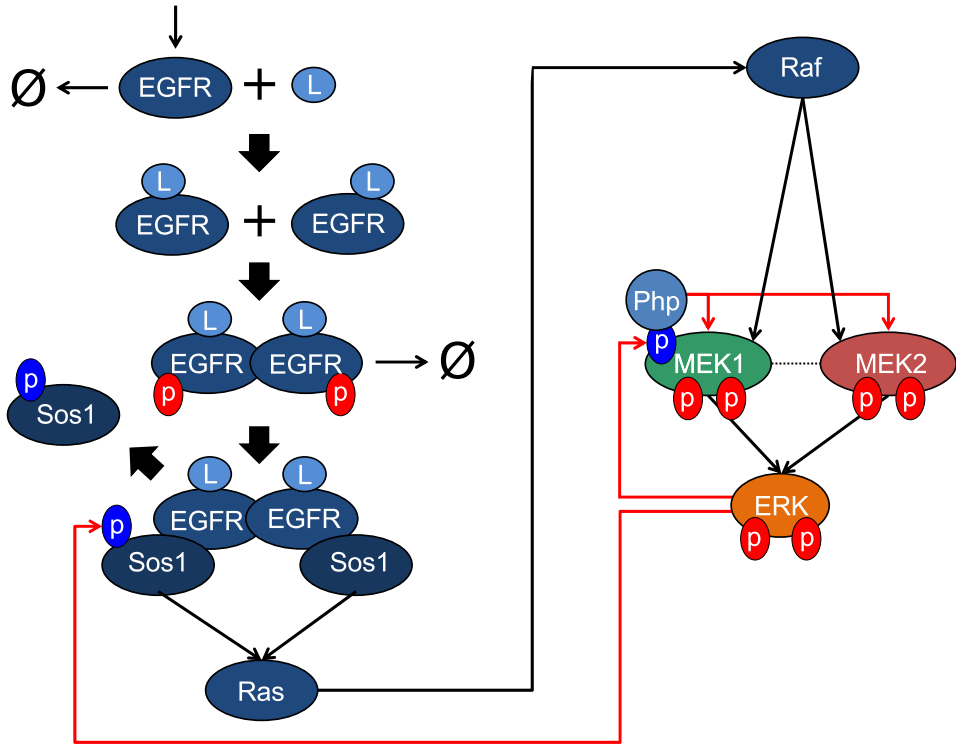

Figure 1. The graphical representation of the ERK cascade model. The growth factor ligands (L) binding to the EGF receptor induces its dimerization, transphosphorylation and subsequent recruitment of Sos1. The receptor-Sos1 complex catalyzes Ras-GDP to Ras-GTP transition, enabling Ras to activate Raf kinase. Activated Raf activates MEK1 and MEK2 by phosphorylating them at their two Raf-dependent sites (RDS). Bisphosphorylated MEK1 and MEK2 phosphorylate ERK; bisphosphorylated ERK is considered the output of the pathway. The red arrows represent two negative feedback loops: (1) active ERK phosphorylates Sos1, preventing its association with the EGFR receptor and (2) active ERK phosphorylates MEK1 (at Thr292) creating an additional binding site for the MEK phosphatase (PHP), which dephosphorylates RDS.

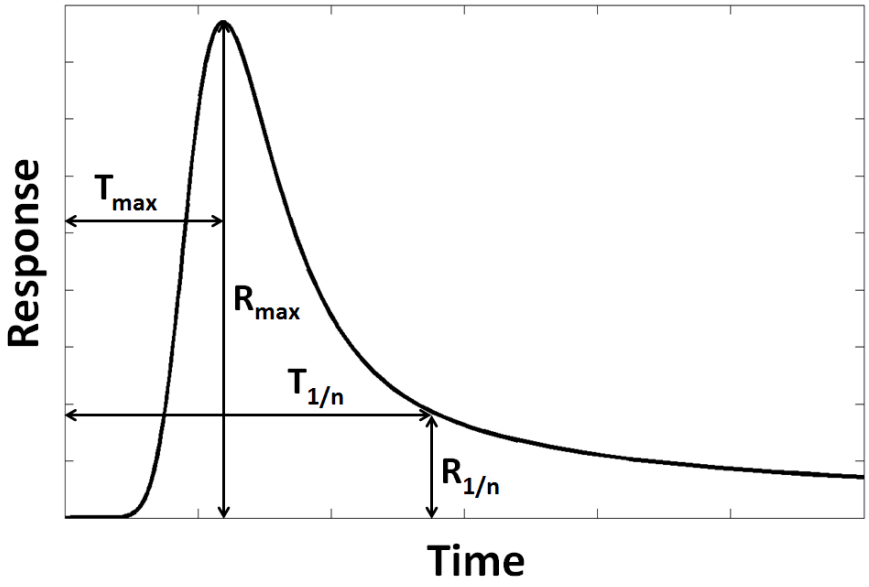

Figure 2. Response metrics. $R_{\max}$ and $T_{\max}$ – the response amplitude and peak time; $T_{1/n}$ – decay time (time required for the response to decrease to $(1/n)$-th of $R_{\max}$, i.e. $R_{1/n}$).

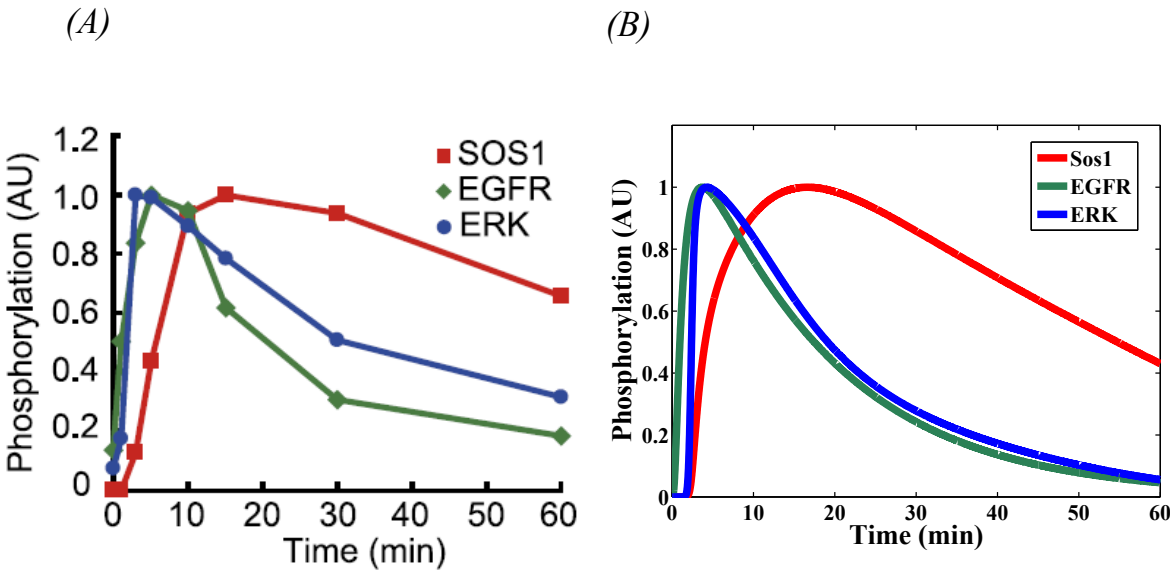

Figure 3. The model validation. (A) the experimental time profiles of (1) the level of EGF receptor phosphorylation, (2) the level of Ras-GTP, and (3) the level of phosphorylated Sos1 due to feedback, Kamioka et al. 2010 [40]. (B) Model predictions.

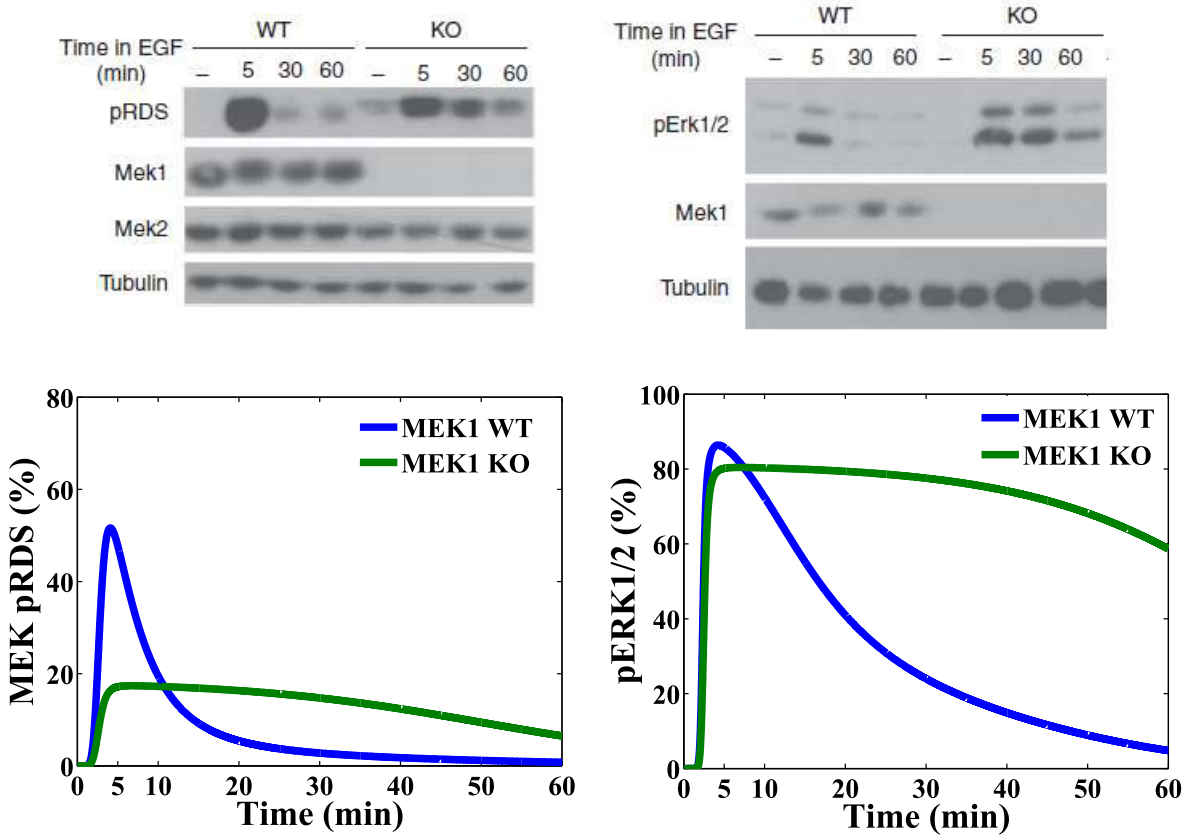

Figure 4. The model validation: the effects of MEK1 knockout (MEK1 KO); upper panel – the experimental results of Catalanotti *et al* [38], lower panel – model predictions. pRDS represents the level of phosphorylation of Raf-dependent phosphorylation sites of both MEK1 and MEK2, reflecting MEK1/2 activation. pERK1/2 refers to the combined level of bisphosphorylated ERK1 and ERK2.

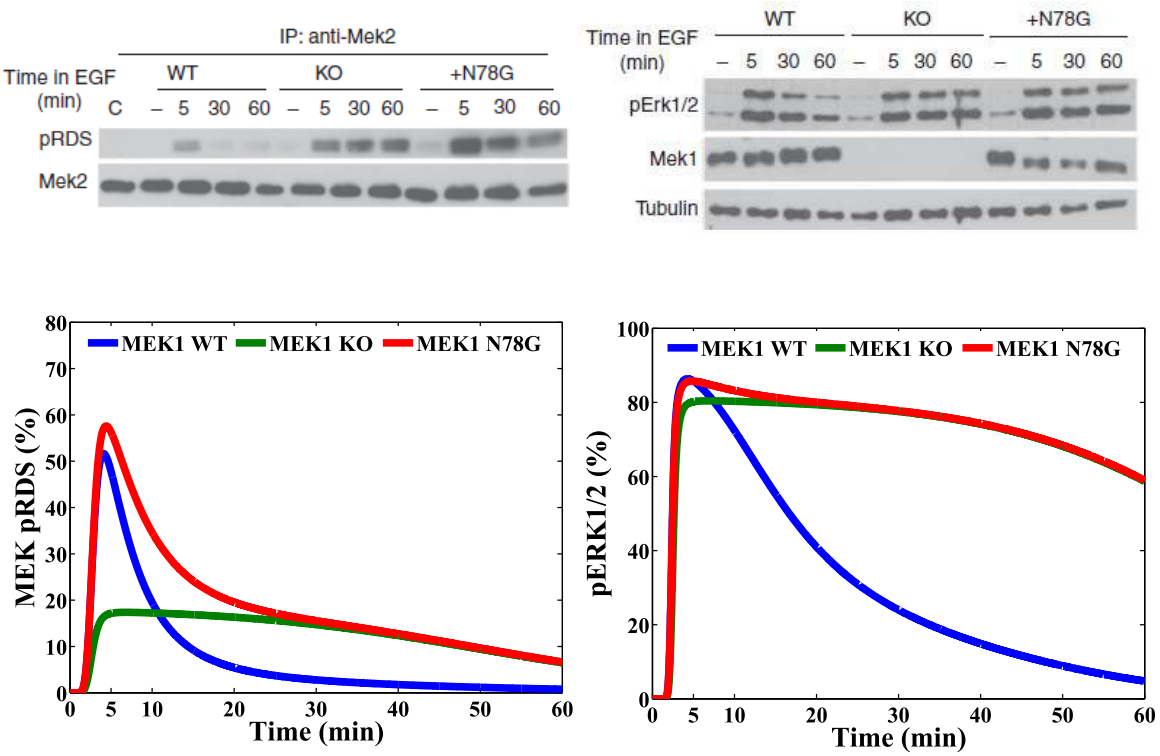

Figure 5. The model validation: the effects of the ablation of MEK1 dimerization (MEK1 mutant N78G); upper panel – the experimental results of Catalanotti *et al* [38], lower panel – model predictions. pRDS represents the level of phosphorylation of Raf-dependent phosphorylation sites of both MEK1 and MEK2. pERK1/2 refers to the combined level of bisphosphorylated ERK1 and ERK2.

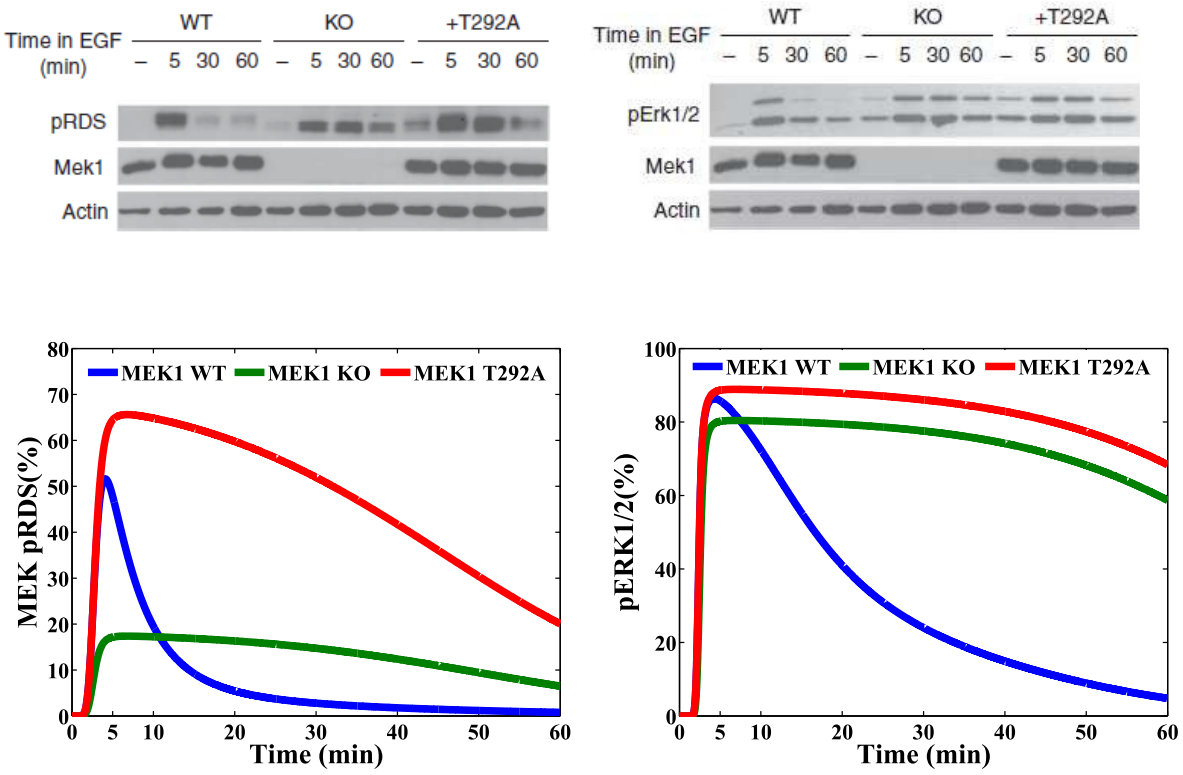

Figure 6. The model validation: the effects of the ablation of the negative feedback site (MEK1 mutant T292A); upper panel – the experimental results of Catalanotti *et al* [38], lower panel – model predictions. pRDS represents the level of phosphorylation of Raf-dependent phosphorylation sites of both MEK1 and MEK2. pERK1/2 refers to the combined level of bisphosphorylated ERK1 and ERK2.

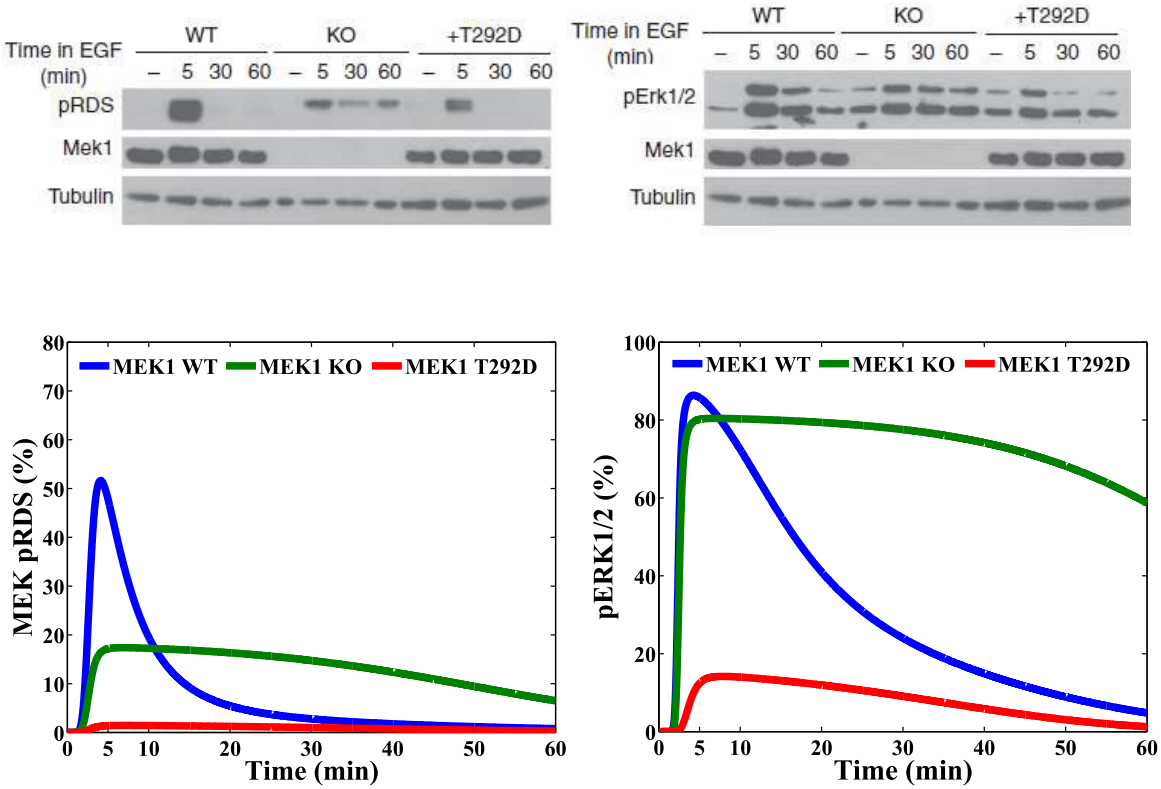

Figure 7. The model validation: the observed and predicted effects of the phosphomimetic mutation of Thr292 (MEK1 mutant T292D); upper panel – the experimental results of Catalanotti *et al* [38], lower panel – model predictions. pRDS represents the level of phosphorylation of Raf-dependent phosphorylation sites of both MEK1 and MEK2. pERK1/2 refers to the combined level of bisphosphorylated ERK1 and ERK2. The predicted MEK pRDS profile for MEK1 T292D cells does not match the observed (see the main text).

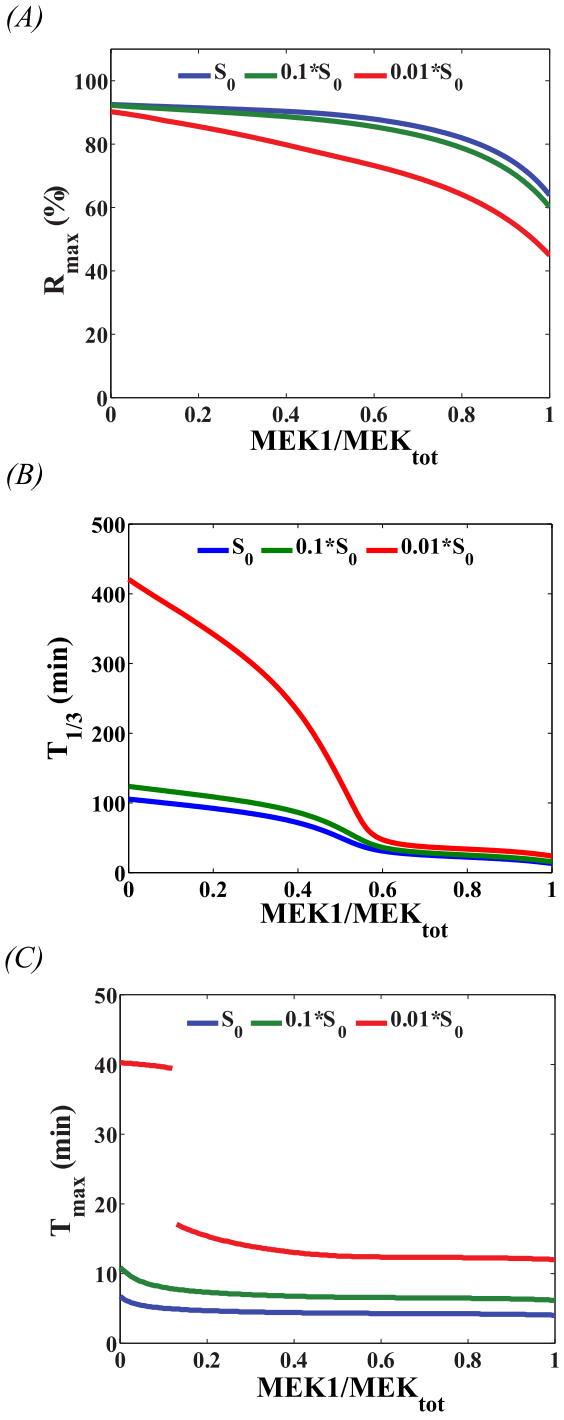

Figure 8. The model predictions: the impact of $MEK1/MEK_{\rm tot}$ ratio on (A) the response amplitude $R_{\rm max}$, (B) decay time $T_{1/3}$, and (C) peak time $\rm T_{max}$. $MEK_{\rm tot}$, the combined amount of MEK1 and MEK2, is kept constant equal to 2×10^5 molecules. S_0 is the default binding rate of the growth factor to the EGFR. There is a discontinuity in the plot on (C). This is due to the existence of two local maxima in time profile; thus time to peak changes abruptly when one maximum becomes higher than the other.

$\mathbf{R_{max}}$	MEK2										
MEK1	10^3	2×10^3	4×10^3	8×10^3	1.6×10^4	3.2×10^4	$\mathbf{6.3\times10^4}$	1.3×10^5	2.5×10^5	5×10^5	10^6
10^3	3	8	17	31	49	66	80	89	94	97	98
2×10^3	4	9	19	32	50	67	80	89	94	97	98
4×10^3	5	11	21	35	51	67	80	89	94	97	98
8×10^3	8	13	23	38	54	68	80	89	94	97	98
1.6×10^4	13	18	28	41	57	70	81	89	94	97	98
3.2×10^4	22	27	35	46	60	73	83	89	94	97	98
6.3×10^4	37	40	45	54	64	75	84	90	94	97	98
$\mathbf{1.3\times10^5}$	54	56	58	63	70	78	**86**	91	95	97	98
2.5×10^5	70	70	72	74	77	82	88	92	95	97	98
5×10^5	82	82	82	83	85	87	90	93	96	98	99
10^6	90	90	90	90	91	91	93	95	96	98	99

$\mathbf{T_{1/3}}$	MEK2										
MEK1	10^3	2×10^3	4×10^3	8×10^3	1.6×10^4	3.2×10^4	$\mathbf{6.3\times10^4}$	1.3×10^5	2.5×10^5	5×10^5	10^6
10^3	48.4	48.0	51.8	59.2	67.1	75.2	84.2	95.1	112.3	> 1000	> 1000
2×10^3	46.5	43.3	45.2	54.7	65.2	74.4	83.8	94.9	112.1	> 1000	> 1000
4×10^3	43.8	39.2	36.5	44.9	61.0	72.7	83.0	94.5	111.7	> 1000	> 1000
8×10^3	38.9	34.6	30.8	31.4	50.3	69.0	81.4	93.6	111.0	> 1000	> 1000
1.6×10^4	31.0	28.6	26.3	25.3	30.2	59.6	78.0	91.8	109.5	> 1000	> 1000
3.2×10^4	22.5	22.1	21.8	21.9	23.3	33.7	69.4	88.1	106.6	> 1000	> 1000
6.3×10^4	16.8	17.2	17.9	19.1	20.8	23.9	42.5	79.4	101.1	> 1000	> 1000
$\mathbf{1.3\times10^5}$	14.2	14.6	15.4	16.8	18.9	21.6	**26.3**	54.1	90.4	130.0	> 1000
2.5×10^5	13.4	13.7	14.3	15.5	17.4	20.2	23.8	30.7	64.7	105.2	> 1000
5×10^5	13.7	14.0	14.4	15.2	16.8	19.3	22.8	27.5	38.3	74.5	> 1000
10^6	14.9	15.0	15.3	15.9	17.1	19.2	22.6	27.3	34.8	51.0	85.1

$\mathbf{T_{max}}$	MEK2										
MEK1	10^3	2×10^3	4×10^3	8×10^3	1.6×10^4	3.2×10^4	$\mathbf{6.3\times10^4}$	1.3×10^5	2.5×10^5	5×10^5	10^6
10^3	7.8	7.3	6.8	6.4	6.2	6.2	6.3	6.4	6.5	6.6	6.7
2×10^3	7.5	6.9	6.4	6.0	5.8	5.8	5.9	6.2	6.4	6.5	6.6
4×10^3	7.1	6.6	6.1	5.7	5.5	5.4	5.6	5.8	6.1	6.3	6.5
8×10^3	6.6	6.2	5.8	5.4	5.1	5.1	5.2	5.4	5.7	6.0	6.3
1.6×10^4	5.9	5.7	5.5	5.2	4.9	4.8	4.9	5.0	5.3	5.7	6.0
3.2×10^4	5.3	5.2	5.1	4.9	4.7	4.6	4.6	4.7	4.9	5.3	5.6
6.3×10^4	4.7	4.7	4.7	4.6	4.5	4.4	4.4	4.5	4.6	4.9	5.2
$\mathbf{1.3\times10^5}$	4.3	4.3	4.3	4.3	4.3	4.3	**4.3**	4.3	4.4	4.6	4.9
2.5×10^5	3.9	3.9	4.0	4.0	4.0	4.1	4.1	4.2	4.2	4.3	4.6
5×10^5	3.7	3.7	3.8	3.8	3.8	3.9	4.0	4.1	4.1	4.2	4.3
10^6	3.6	3.6	3.6	3.7	3.7	3.7	3.8	3.9	4.0	4.1	4.2

Figure 9. The impact of the MEK1 and MEK2 levels (given in numbers of molecules per cell) on the amplitude $R_{\max}$ (given in %), the decay time $T_{1/3}$ (given in minutes), and the peak time $T_{\max}$ (given in minutes). Color is used to show the main trend. The rectangle marks the default MEK1 and MEK2 levels.

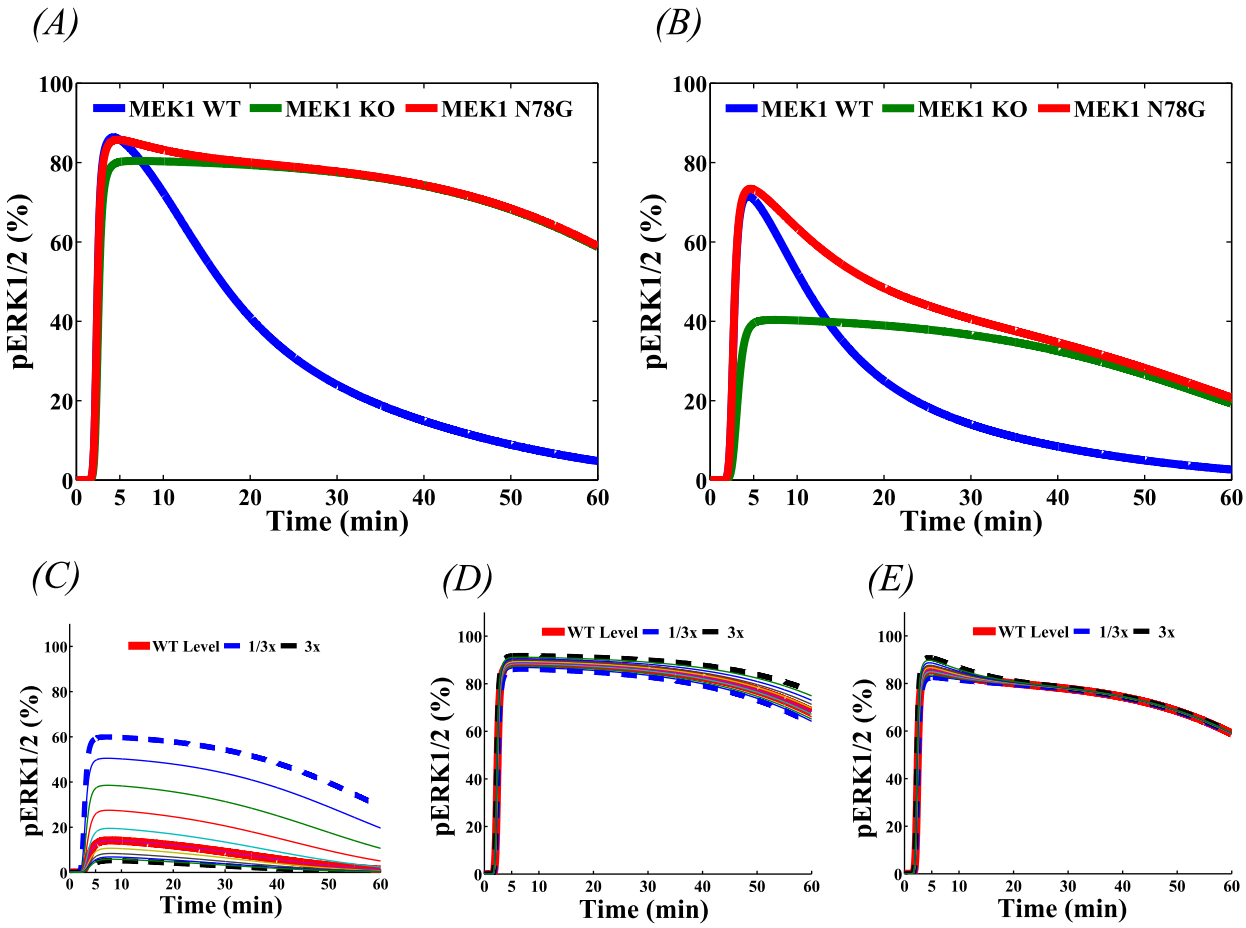

Figure 10. The model predictions. Upper panels: the estimation of the MEK2/MEK1 catalytic activity ratio. (*A*) response profiles obtained after assuming that catalytic activity of MEK2 is equal to the catalytic activity of MEK2. (*B*) response profiles obtained after assuming MEK2/MEK1 activity ratio equal to 5 (default parameter values in the model). The latter profile agrees with the experiment (see figure 5). Lower panels: sensitivity of cell mutants responses to the level of expression of the MEK1 mutant expressed in MEK1 KO cells. The time profiles of bisphosphorylated ERK in the cells transfected with MEK1 mutant with expression varying in 3-fold range in respect to the expression of WT MEK1. (*C*) T292A transfectants, (*D*) N78G transfectants, and (*E*) T292A transfectants.

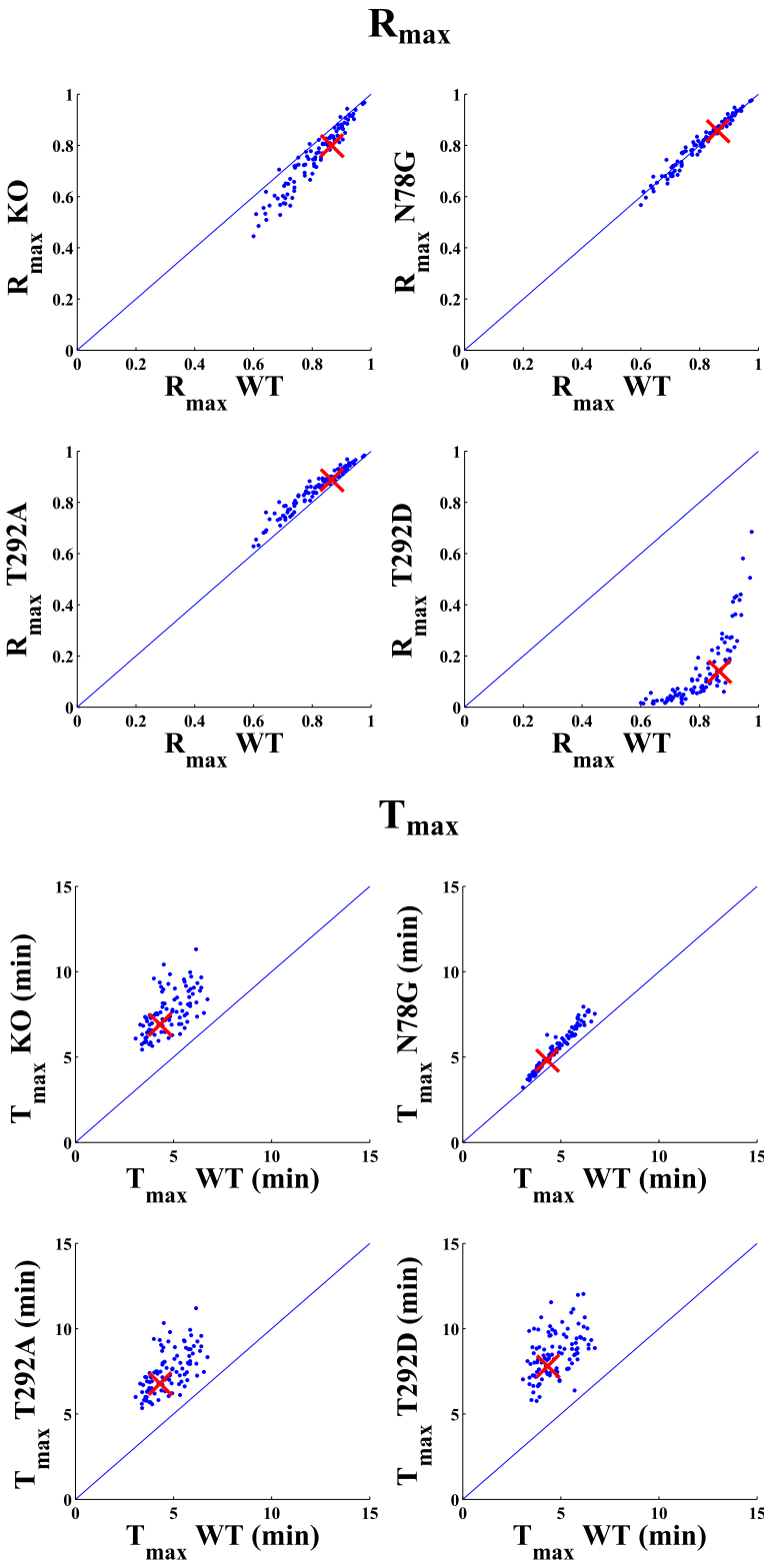

Figure 11. Upper four panels: time to peak $T_{\max}$, and lower four panels: relative response amplitude $R_{\max}$, for WT cells versus four cell mutants, calculated for 100 parameters sets representing *a posteriori* distribution, see Appendix for details. The crosses correspond to the default parameter set given in Table 1.

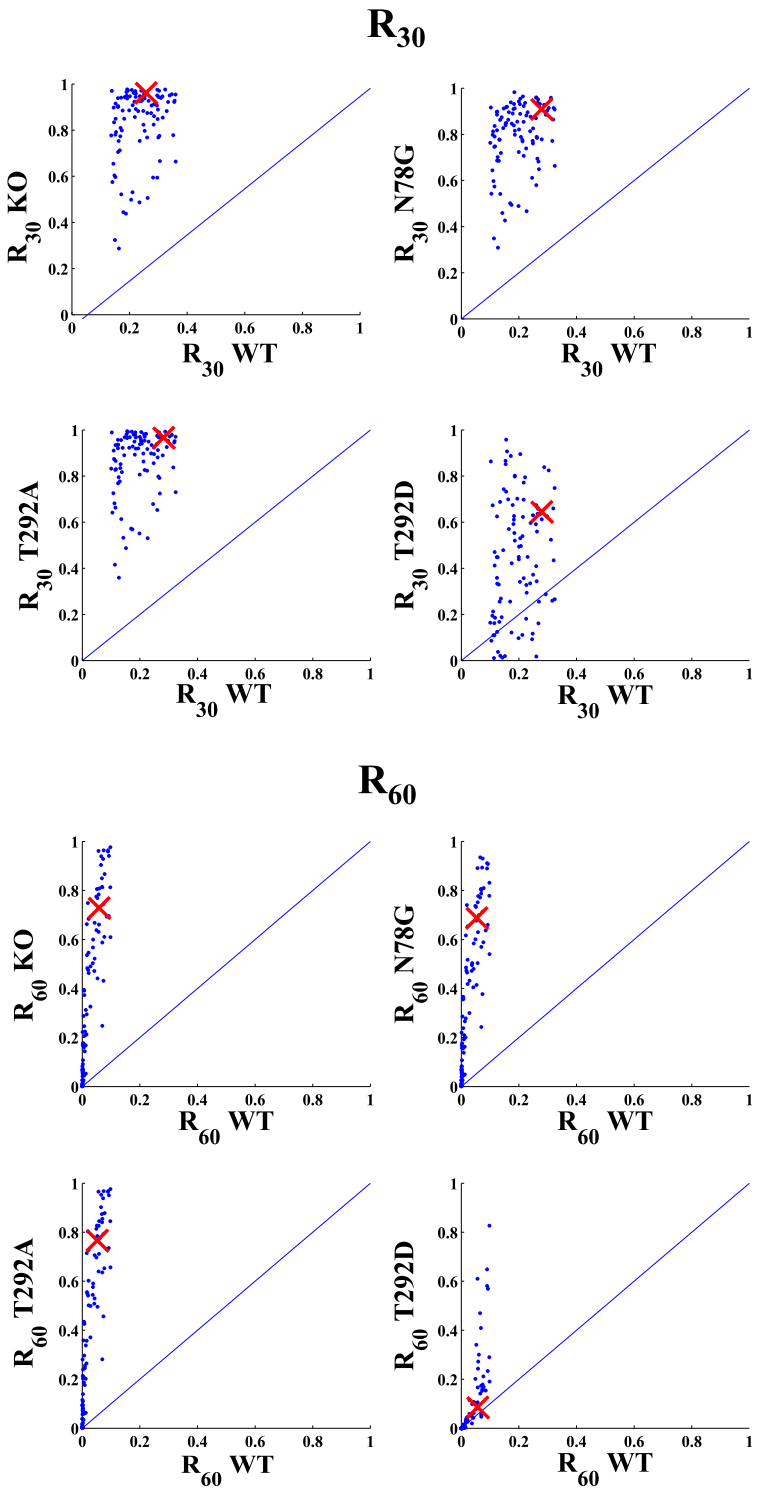

Figure 12. Upper four panels: response at 30 min R_{30}, and lower four panels: response at 60 min R_{60}, for WT cells versus four cell mutants, calculated for 100 parameters sets representing *a posteriori* distribution, see Appendix for details. The cross corresponds to the default parameter set given in Table 1.

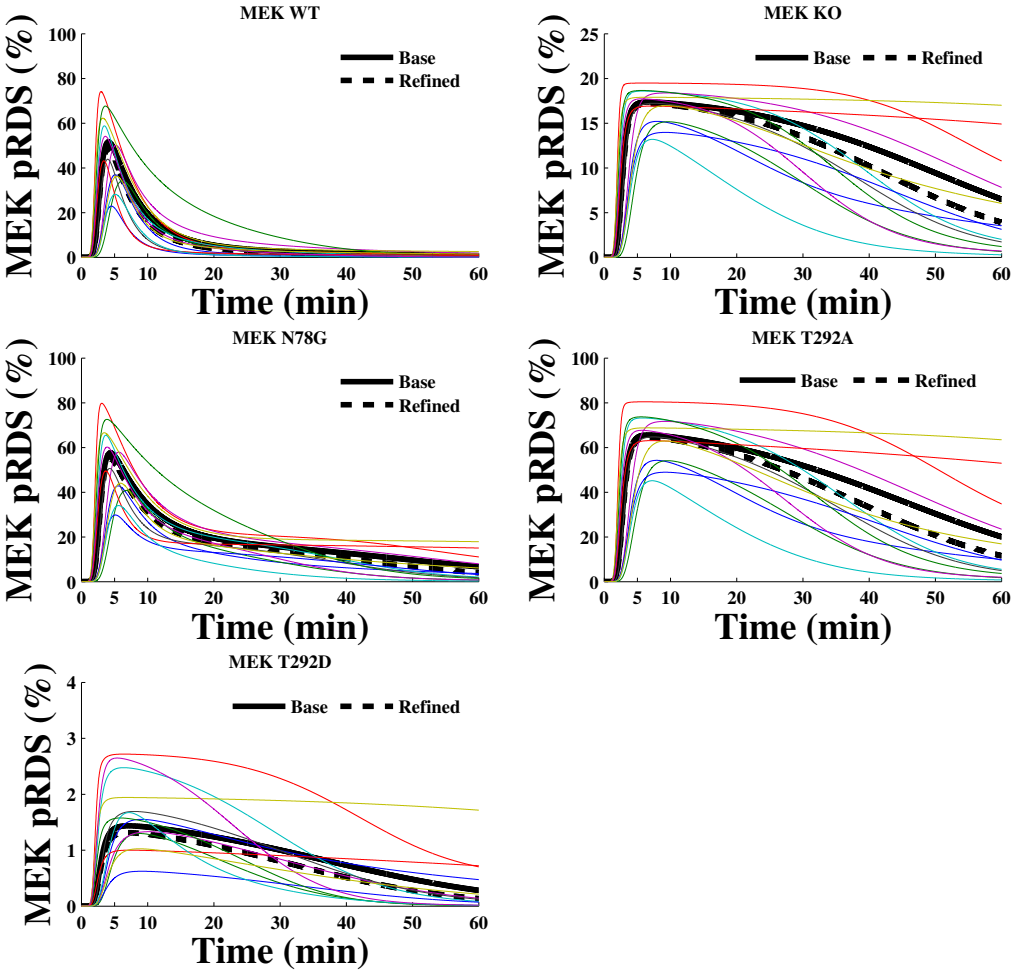

Figure 13. Bisphosphorylated MEK_{pp} time profiles. Thin (color) lines correspond to 13 parameter sets sampled from *a posteriori* distribution, bold line and dashed bold line correspond to default parameters and to refined parameters (averaged over the *a posteriori* distribution), respectively, given in Table 1.

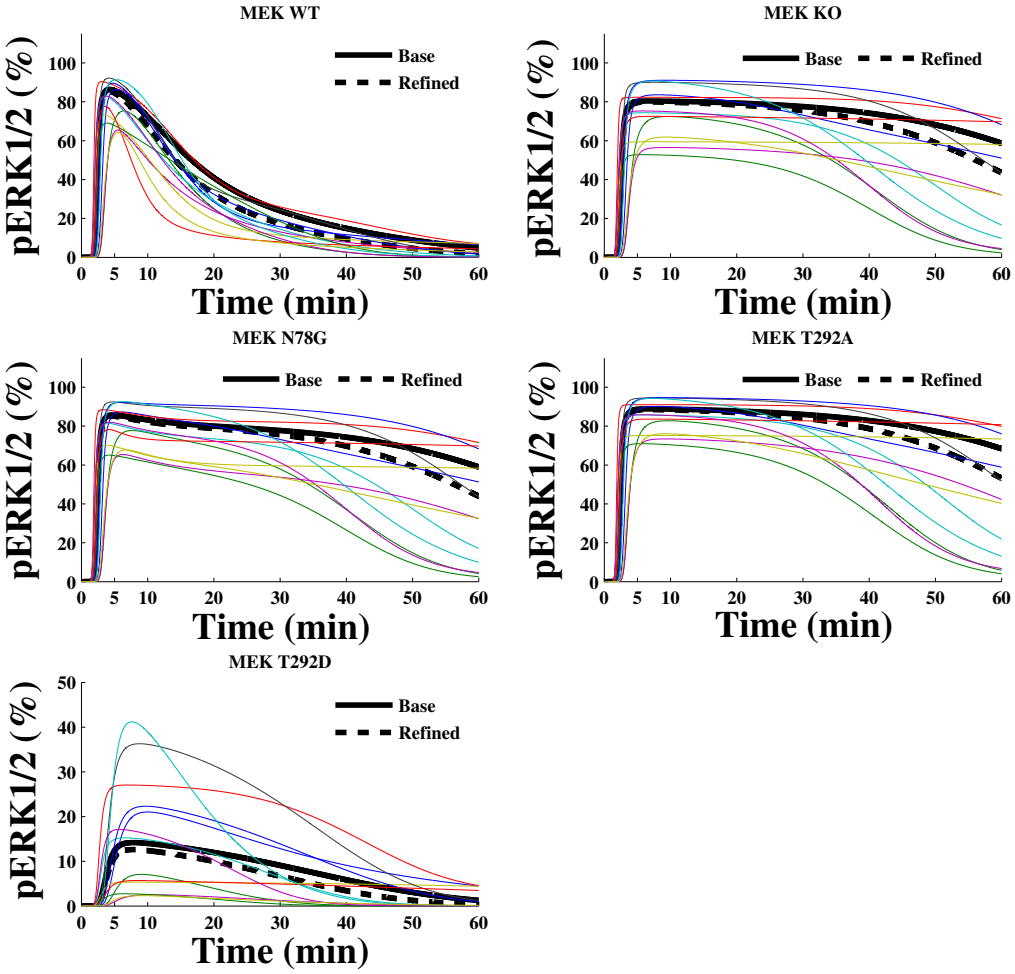

Figure 14. Bisphosphorylated ERK_{pp} time profiles. Thin lines correspond to 13 parameter sets sampled from *a posteriori* distribution, bold line and dashed bold line correspond to default parameters and to refined parameters (averaged over the *a posteriori* distribution), respectively, given in Table 1.

Parameter	**Symbol**	**Default Value**	**Refined Value**	**Affected Metric**
Ligand–EGFR complex dimerization	c_2	2×10^{-7} $(\text{mcls} \times \text{s})^{-1}$	1.97×10^{-7}	$T^+_{\max}$
EGFR dimer transphosphorylation	t_1	100 s^{-1}	98	
EGFR dimer degradation	d_3	10^{-3} s^{-1}	1.20×10^{-3}	R^-_{30}, R^-_{60}
EGFR–Sos1 association	b_1	4×10^{-8} $(\text{mcls} \times \text{s})^{-1}$	3.99×10^{-8}	$T^-_{\max}$, R^+_{60}
EGFR–Sos1 dissassociation	n_1	2×10^{-3} s^{-1}	2.03×10^{-3}	R^-_{60}
Ras activation by EGFR-Sos1	a_1	1.5×10^{-7} $(\text{mcls} \times \text{s})^{-1})$	1.45×10^{-7}	$\text{T}^-_{\max}$,R^+_{30},R^+_{60}
Ras inactivation	i_1	2×10^{-2} s^{-1}	2.00×10^{-2}	$T^+_{\max}$,R^-_{30},R^-_{60}
Raf activation by Ras	a_2	4×10^{-8} $(\text{mcls} \times \text{s})^{-1}$	3.93×10^{-8}	$R^+_{\max}$,$T^-_{\max}$,R^+_{30},R^+_{60}
Raf inactivation	i_2	10^{-2} s^{-1}	1.00×10^{-2}	$R^-_{\max}$,R^-_{30},R^-_{60}
MEK1/2 phosphorylation by Raf	p_1	1.5×10^{-7} $(\text{mcls} \times \text{s})^{-1}$	1.46×10^{-7}	$R^+_{\max}$,$T^-_{\max}$,R^+_{30},R^+_{60}
MEK1/2 dephosphorylation	u_1	5.0×10^{-3} s^{-1}	5.11×10^{-3}	$R^-_{\max}$,R^-_{30},R^-_{60}
Phosphorylation of ERK by MEK1	$p_{2\text{a}}$	10^{-6} $(\text{mcls} \times \text{s})^{-1}$	1.00×10^{-6}	
Phosphorylation of ERK by MEK2	$p_{2\text{b}}$	5×10^{-6} $(\text{mcls} \times \text{s})^{-1}$	5.01×10^{-6}	$R^+_{\max}$,R^+_{30},R^+_{60}
Dephosphorylation of ERK	u_2	2×10^{-2} s^{-1}	2.03×10^{-2}	$R^-_{\max}$,R^-_{30},R^-_{60}
Sos1 phosphorylation by ERK	p_3	2×10^{-3} $(\text{mcls} \times \text{s})^{-1}$	2.01×10^{-3}	
Sos1 dephosphorylation (FB)	u_3	1×10^{-3} $(\text{mcls} \times \text{s})^{-1}$	1.00×10^{-3}	R^+_{60}
MEK1 phosphorylation by ERK	p_4	1.2×10^{-9} $(\text{mcls} \times \text{s})^{-1}$	1.46×10^{-9}	$T^-_{\max}$, R^-_{30}, R^-_{60}
MEK1 dephosphorylation (FB)	u_4	2×10^{-4} $(\text{mcls} \times \text{s})^{-1}$	1.95×10^{-4}	R^+_{60}
PHP–MEK1 binding	b_5	4×10^{-9} $(\text{mcls} \times \text{s})^{-1}$	4.27×10^{-9}	$T^-_{\max}$,R^-_{30},R^-_{60}
PHP–MEK1 dissassociation	n_5	2×10^{-4} s^{-1}	1.88×10^{-4}	R^+_{30},R^+_{60}
MEK1 dephosphorylation (PHP)	u_5	20 s^{-1}	21	
EGFR monomer synthesis	s_1	2.5 s^{-1}	N/A	N/A
EGFR monomer degradation	d_1	5×10^6 s^{-1}	N/A	N/A
Sos1 synthesis	s_2	1 s^{-1}	N/A	N/A
Sos1 degradation	d_2	5×10^6 s^{-1}	N/A	N/A
Ligand–EGFR binding, signal S_0	c_1	0.02	N/A	N/A
MEK1 homodimerization	b_2	10^{-5} $(\text{mcls} \times \text{s})^{-1}$	N/A	N/A
MEK1 dimer dissassociation	n_2	10^{-3} s^{-1}	N/A	N/A
MEK2 homodimerization	b_3	10^{-5} $(\text{mcls} \times \text{s})^{-1}$	N/A	N/A
MEK2 dimer dissassociation	n_3	3×10^{-2} s^{-1}	N/A	N/A
MEKs heterodimerization	b_4	10^{-5} $(\text{mcls} \times \text{s})^{-1}$	N/A	N/A
MEKs heterodimer dissassociation	n_4	10^{-3} s^{-1}	N/A	N/A

Table 1. Kinetic parameters. Unless stated otherwise, figures are plotted for default parameters, and these parameters are used in BioNetGen codes included in the Electronic Supplementary Material. The refined parameters are parameters averaged over the *a posteriori* distribution, see Appendix for details. The time to peak $T_{\max}$ is considered affected by a given parameter when 10-fold change of the parameter (either below or above its default value) results in at least fd = 0.8 fold change (increase or decrease) of $T_{\max}$. Annotations $T^-_{\max}$ or $T^+_{\max}$ in the last column imply that the time to peak is affected by a given parameter, while the sign in the superscript denotes positive or negative influence. The same convention is used for the other three metrics $R_{\max}$, R_{30} and R_{60}, although for the last two metrics the fd values are chosen, respectively, 0.7 and 0.5.

Species	Default	HeLa [40]	Hepatocytes [11]	HeLa [12]	CHO [53]	PC12 [16]
EGFR	0.5	0.42	0.1	0.03	0.08	0.3
Sos1	0.2	0.12	0.034	0.04	0.01	0.1
Ras	0.5	0.43	N/A	7.1	0.12	0.1
Raf	0.5	0.012	N/A	0.025	0.1	0.7
MEK (tot)	0.2	1.4	N/A	13.6	0.12	0.68
MEK1	0.133	N/A	N/A	N/A	N/A	N/A
MEK2	0.067	N/A	N/A	N/A	N/A	N/A
ERK	3	0.96	N/A	13.0	0.024	0.26
PHP (MEK)	3	N/A	N/A	0.025	0.0114	0.018

Table 2. Species concentrations. The species concentrations are given in μM for the sake of comparison with the other models. The conversion of mlcl/cell to cytoplasmic concentrations was assumed to be 10^6 mcls = 1μM, equivalent to cell volume of 2000 μm^3 with 1/6 occupied by the nucleus.